# An organic spiking artificial neuron with excitatory and inhibitory synapses: towards soft and flexible organic neuromorphic processing

Mohammad Javad Mirshojaeian Hosseini[1,2], Yi Yang[1,3], Simeon Bamford[4], Chiara Bartolozzi[4], Giacomo Indiveri[5], Robert A. Nawrocki[1,4*]

[1]School of Engineering Technology, Purdue University, 401 S Grant St, West Lafayette, Indiana, 47906, USA.
[2]Department of chemical Engineering, Stanford University, 443 Via Ortega, Stanford, 94305, CA, USA.
[3]Department of Mechanical and Automation Engineering, The Chinese University of Hong Kong, University Ave, Ma Liu Shui, Hong Kong, China.
[4]Event-Driven Perception for Robotics, Italian Institute of Technology, Via San Quirico 19d, 16163 Genova, Italy.
[5]Institute of Neuroinformatics, University of Zurich and ETH Zurich, Winterthurerstrasse 190, 8057 Zürich, Switzerland.

*Corresponding author(s). E-mail(s): robertnawrocki@purdue.edu;
Contributing authors: mjmir@stanford.edu; yeeyoung1993@gmail.com; simeon.bamford@iit.it; chiara.bartolozzi@iit.it; giacomo@ini.uzh.ch;

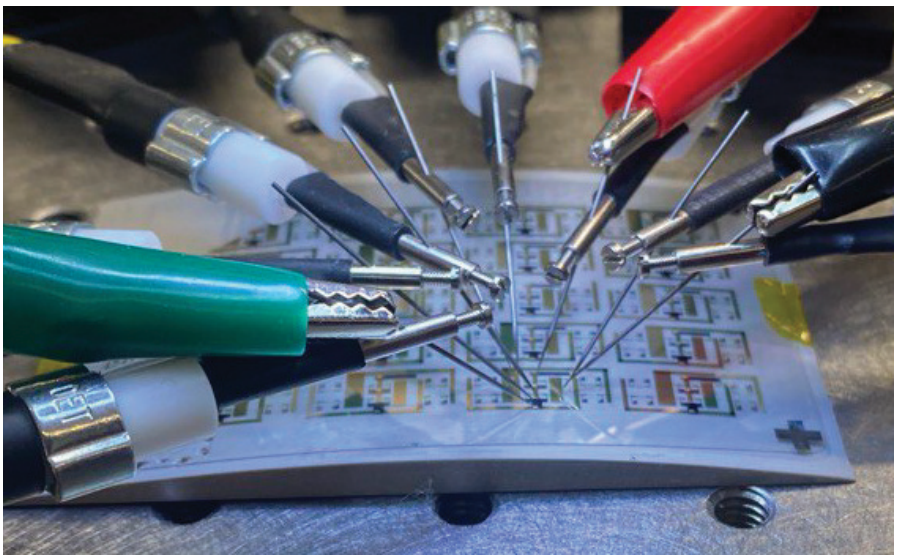

**Supplementary Figure 1** Photograph of the flexible spiking neuron circuit under bent configurations. Demonstrates mechanical flexibility of the fabricated circuit, showing structural integrity and device layout consistency across bending. The bending radius is 205 mm.

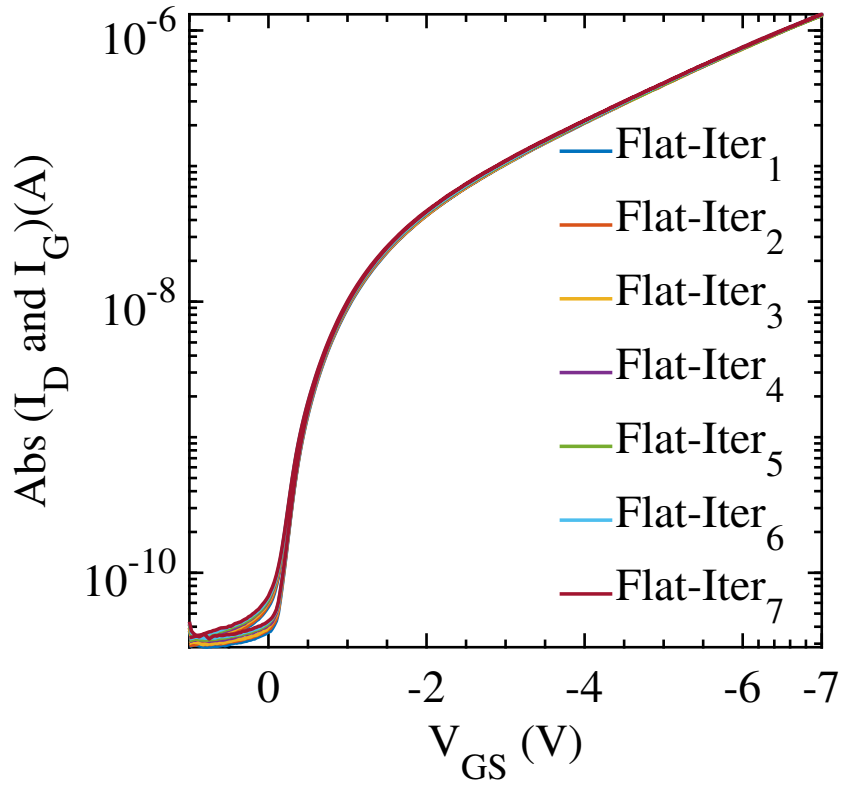


**Supplementary Figure 2** Stress test of p-type OFETs across seven consecutive measurements. Transfer characteristics remain stable, indicating high electrical reliability and robustness under repeated operation.

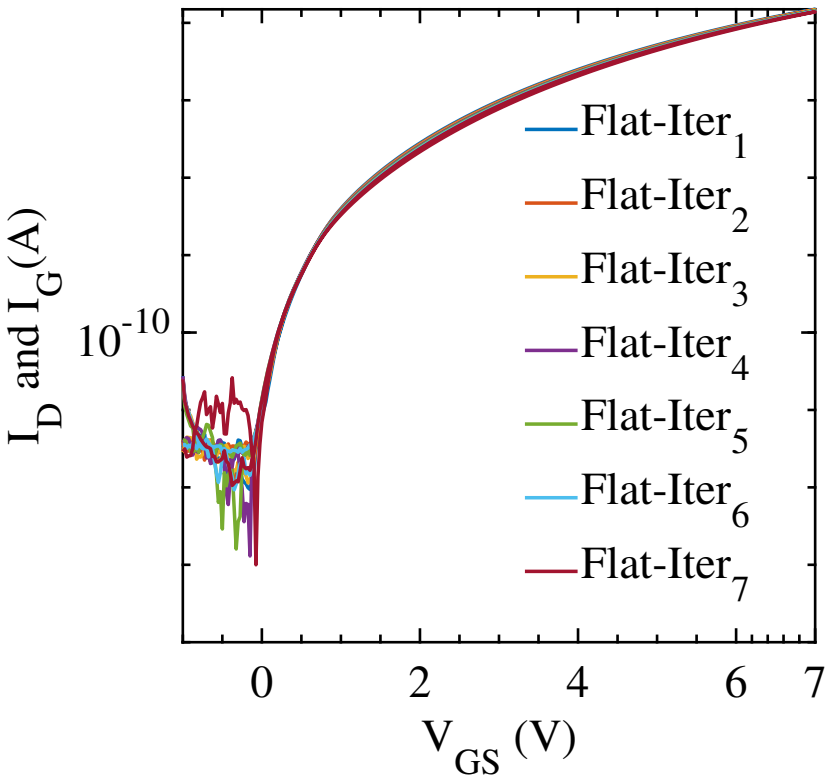


**Supplementary Figure 3** Stress test of n-type OFETs across seven consecutive measurements. Device behavior is consistent across cycles, indicating high electrical reliability and robustness under repeated operation.

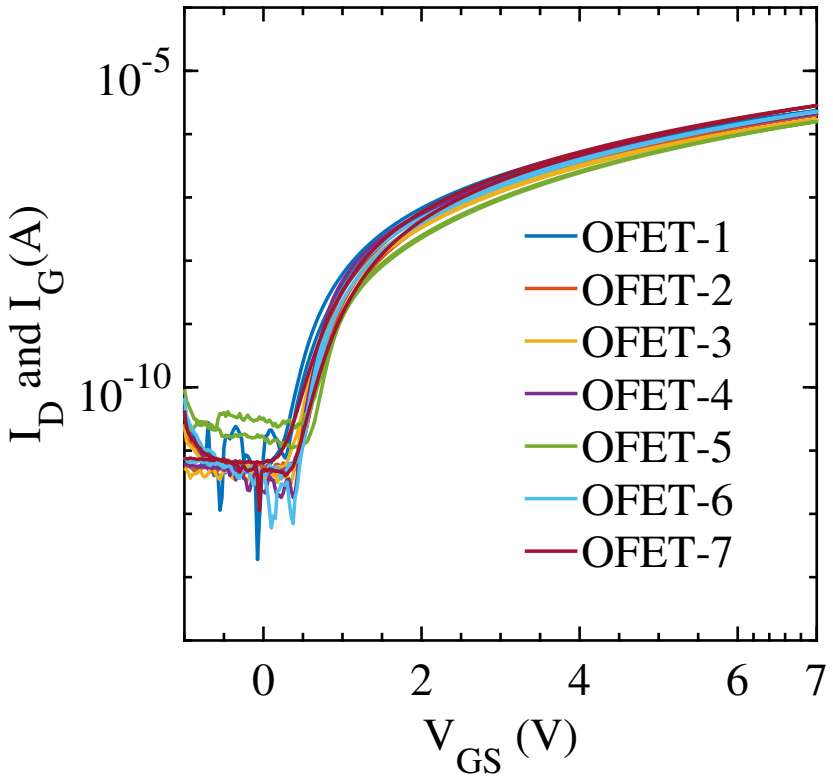


**Supplementary Figure 4** Device-to-device variability of n-type OFETs across a single chip.

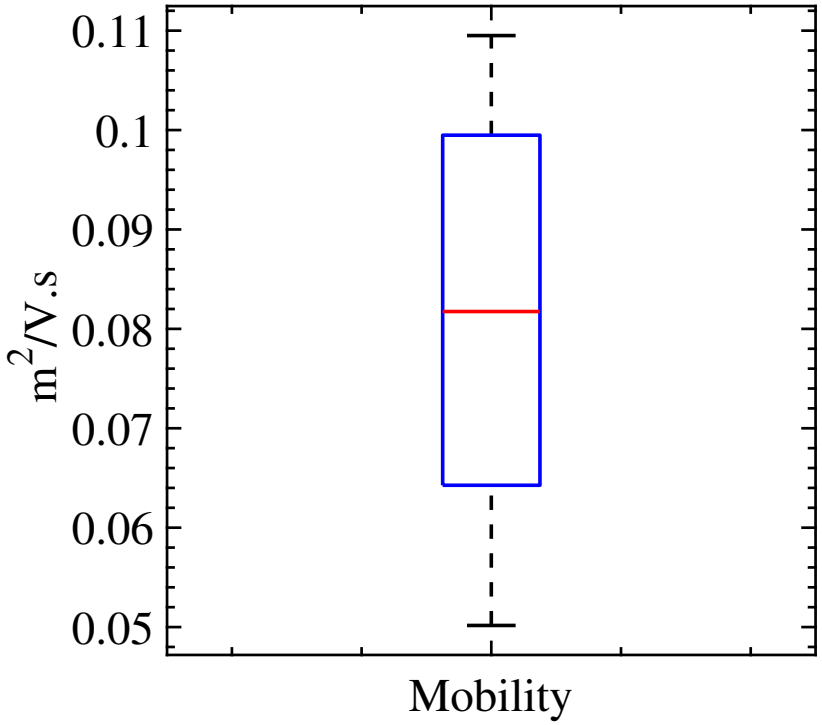


**Supplementary Figure 5** Device-to-device mobility variability of n-type OFETs across a single chip.

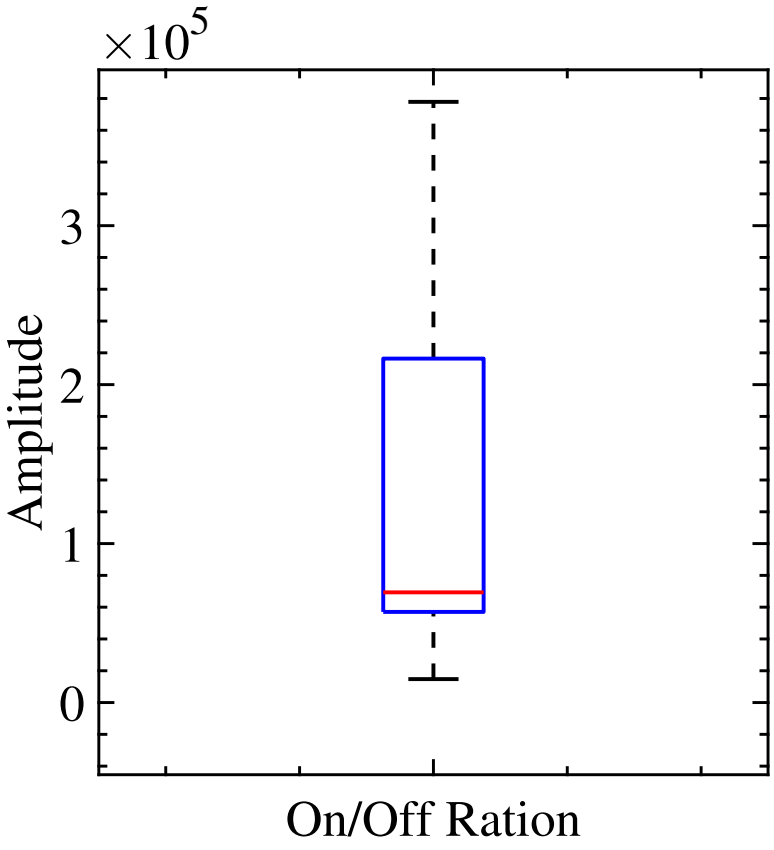


**Supplementary Figure 6** Device-to-device on/off ratio variability of n-type OFETs across a single chip.

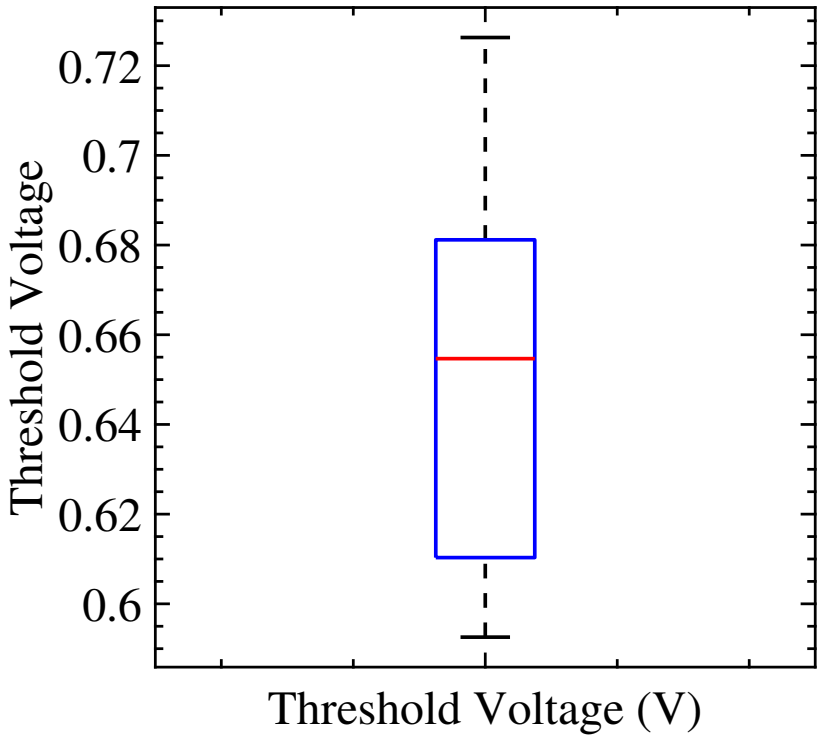


**Supplementary Figure 7** Device-to-device threshold voltage variability of n-type OFETs across a single chip.

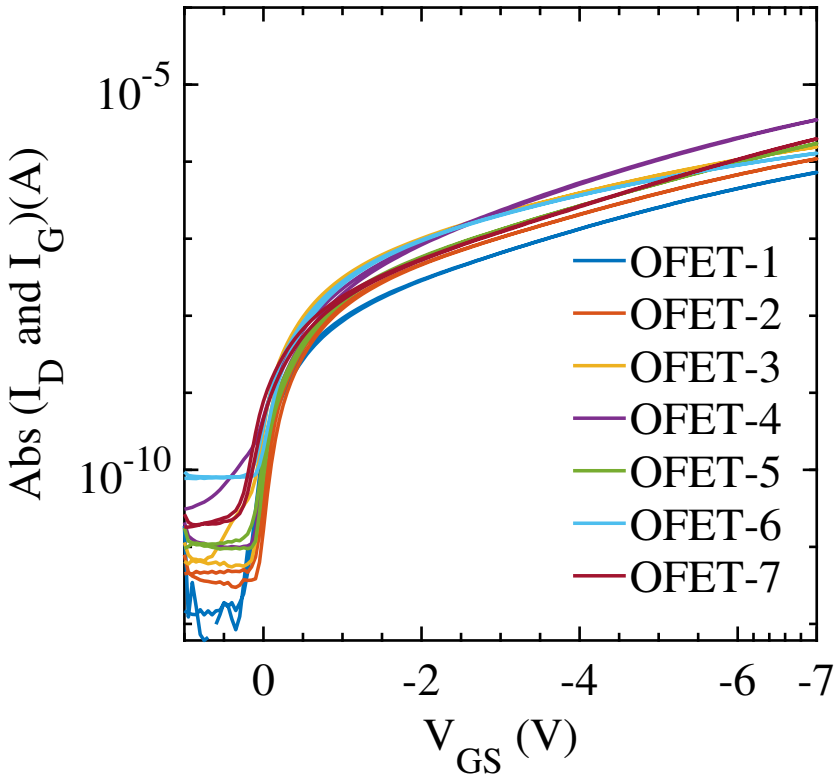


**Supplementary Figure 8** Device-to-device variability of p-type OFETs across a single chip.

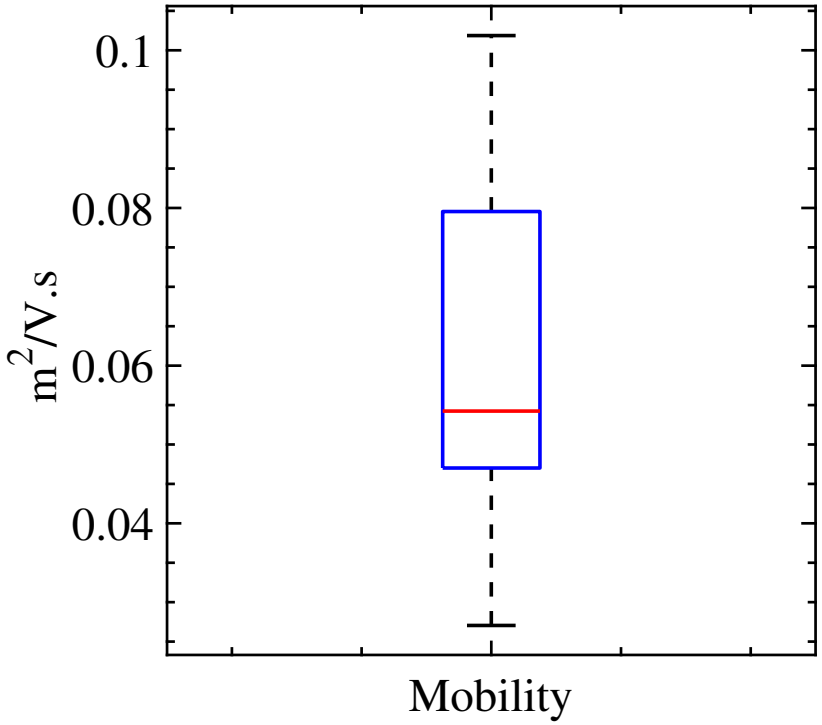


**Supplementary Figure 9** Device-to-device mobility variability of p-type OFETs across a single chip.

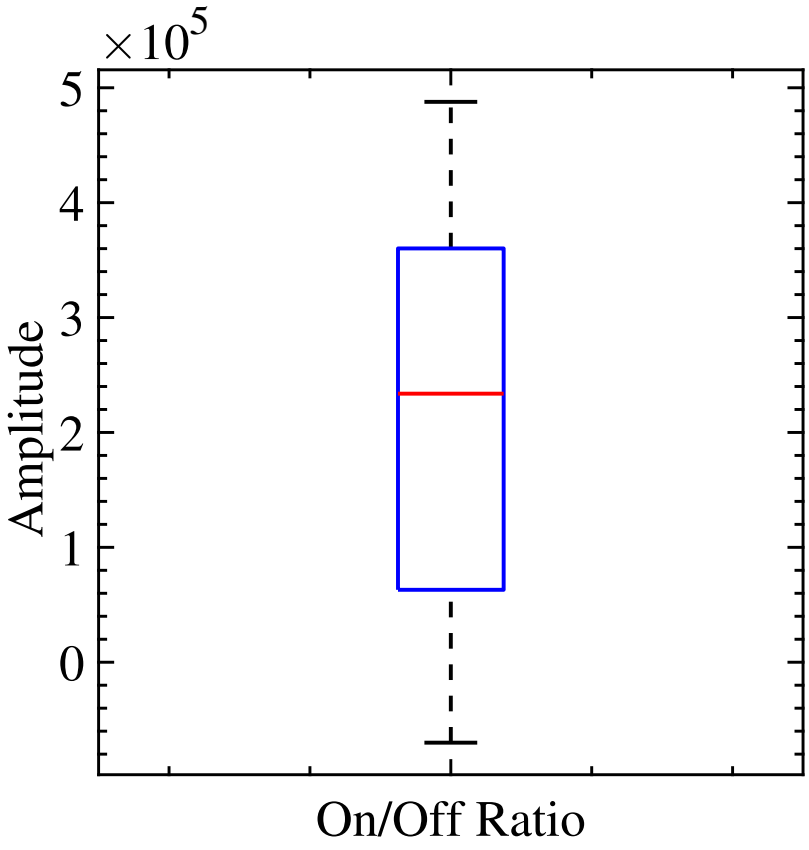


**Supplementary Figure 10** Device-to-device on/off ratio variability of p-type OFETs across a single chip.

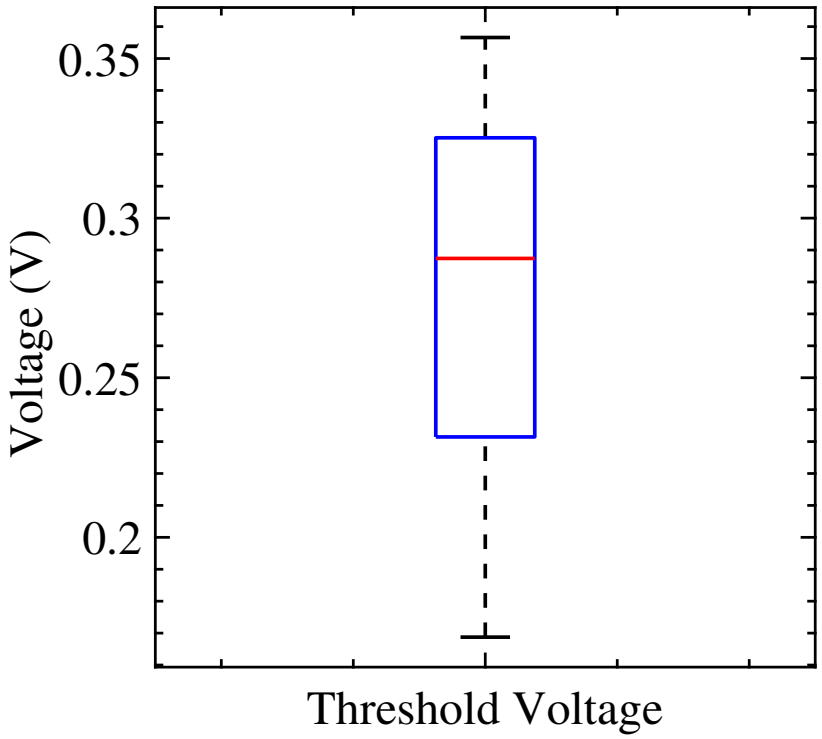


**Supplementary Figure 11** Device-to-device threshold voltage variability of p-type OFETs across a single chip.

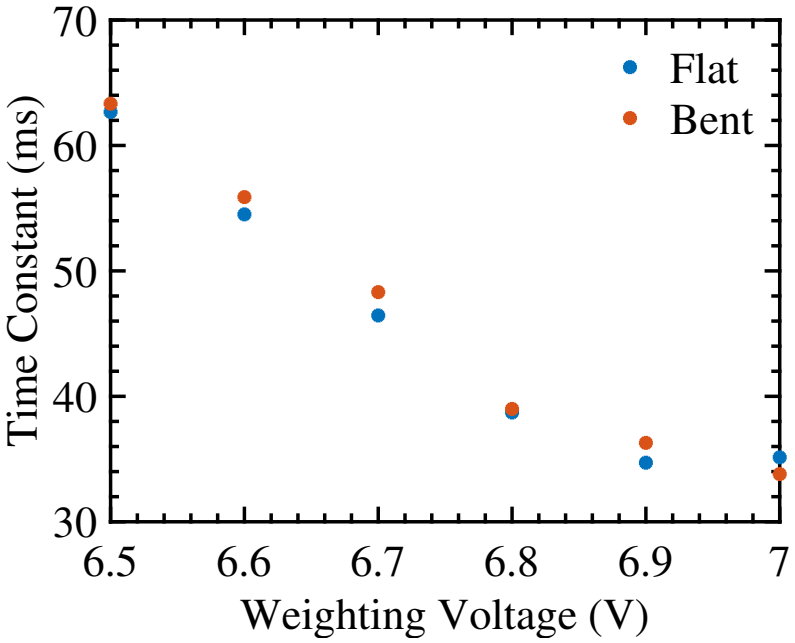


**Supplementary Figure 12** Time constant of excitatory PCS synaptic circuit across weighing voltages in flat and bent states. The time constant decreases with higher weighing voltages. Bending has minimal impact on synaptic temporal dynamics.

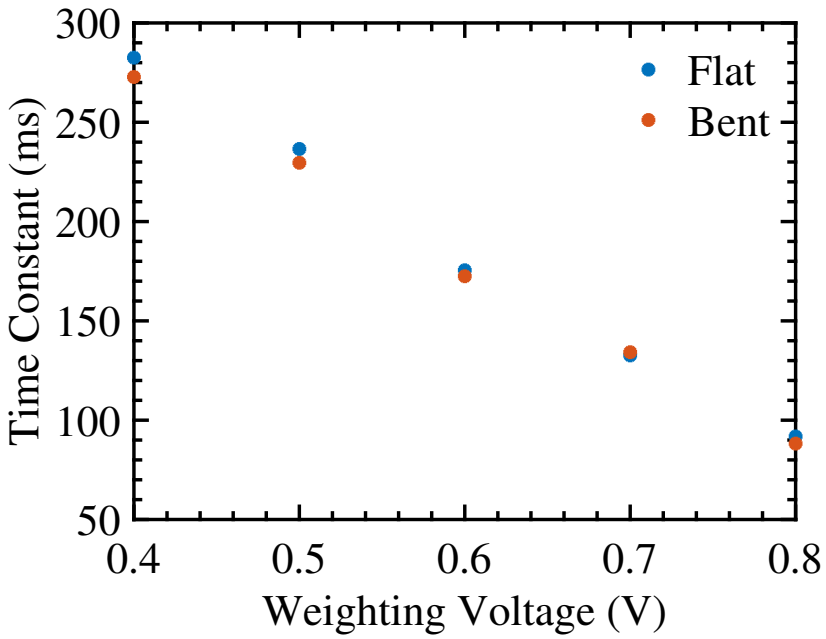


**Supplementary Figure 13** Time constant of inhibitory PCS synaptic circuit across weighing voltages in flat and bent states. Inhibitory synapses maintain high time constants (∼275–280 ms) at low weighing voltages. A slight variation is observed with bending.

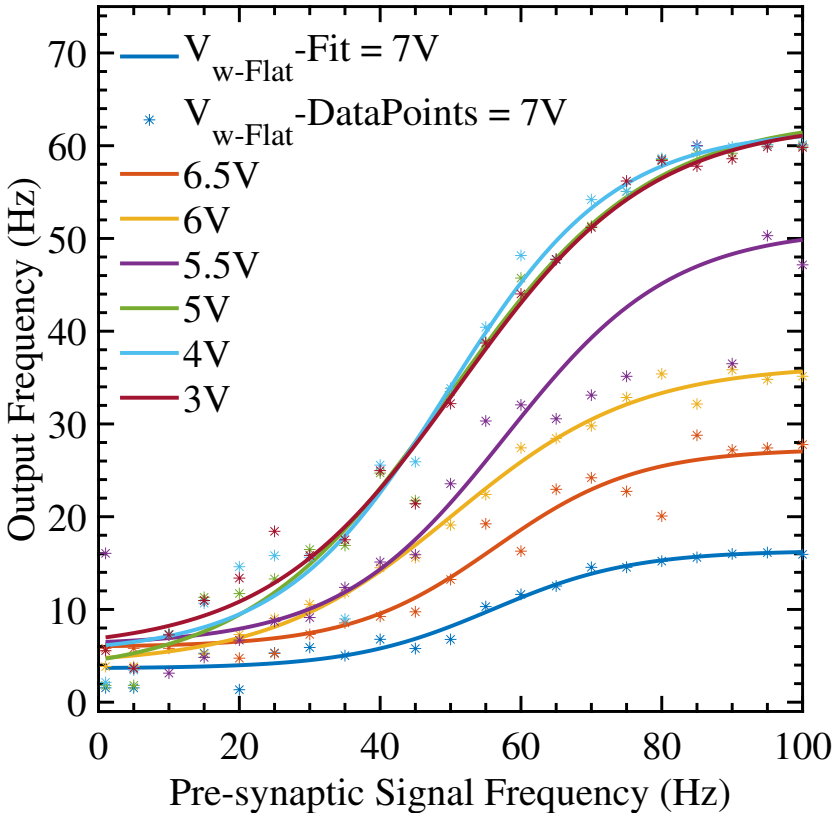


**Supplementary Figure 14** Measured output firing rates of the excitatory synaptic circuit in the flat configuration across eight synaptic weight voltages. Raw data points illustrating the neuron's firing rate response as a function of presynaptic frequency (1–100 Hz). Data corresponds to the fitted sigmoidal curves shown in Figure4a (solid lines).

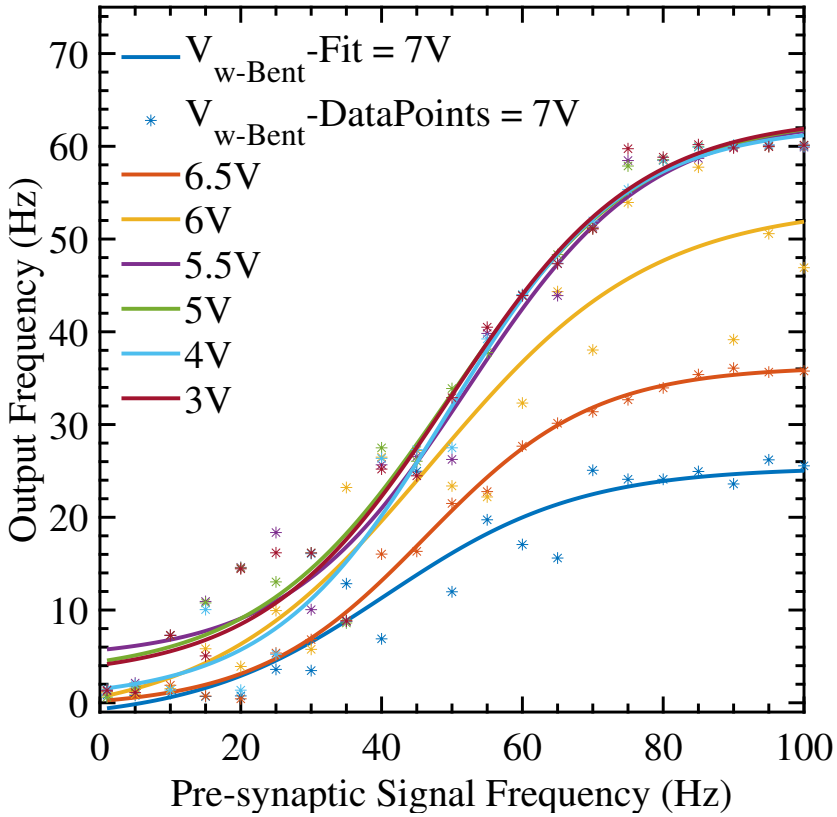


**Supplementary Figure 15** Measured output firing rates of the excitatory synaptic circuit in the bent configuration across eight synaptic weight voltages. Experimental data supporting Figure 4a (dotted lines), showing how mechanical bending influences the spiking response at varying synaptic weights and presynaptic input frequencies.

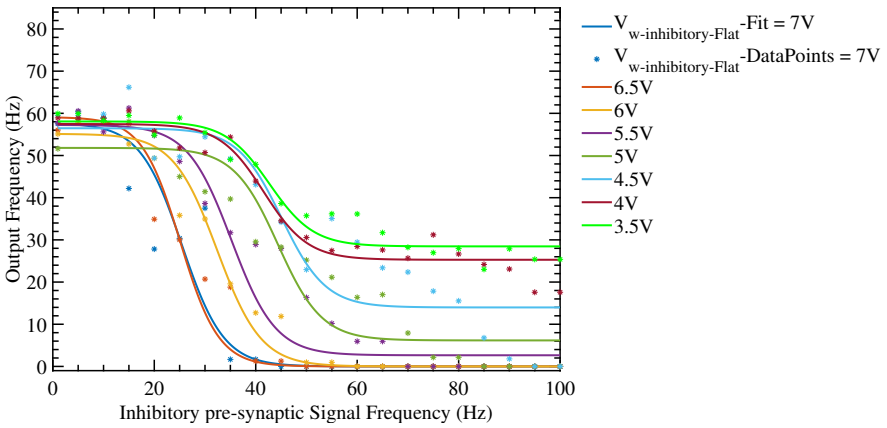


**Supplementary Figure 16** Measured output firing rates of the inhibitory synaptic circuit in the flat configuration across eight synaptic weight voltages. Raw firing rate data corresponding to the inhibitory condition in Figure 4b (solid lines), demonstrating suppression of output spikes as input frequency increases, modulated by synaptic weight.

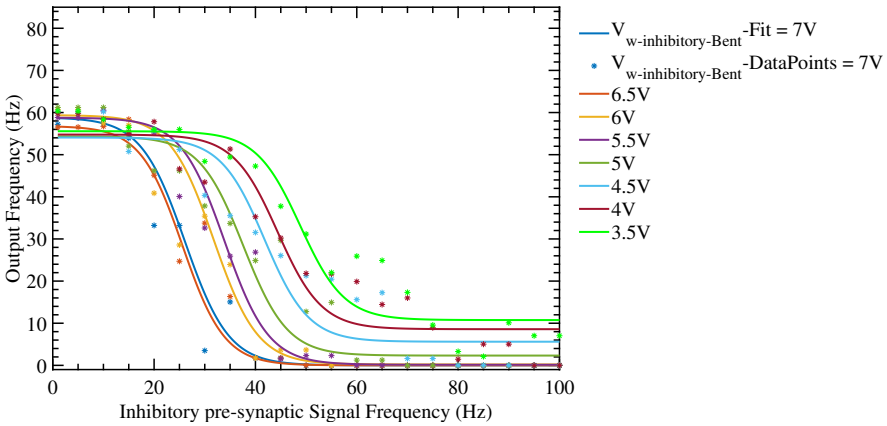


**Supplementary Figure 17** Measured output firing rates of the inhibitory synaptic circuit in the bent configuration across eight synaptic weight voltages. Data matches the fitted curves in Figure 4b (dotted lines), highlighting the impact of mechanical strain on inhibitory response shaping in organic spiking neurons.

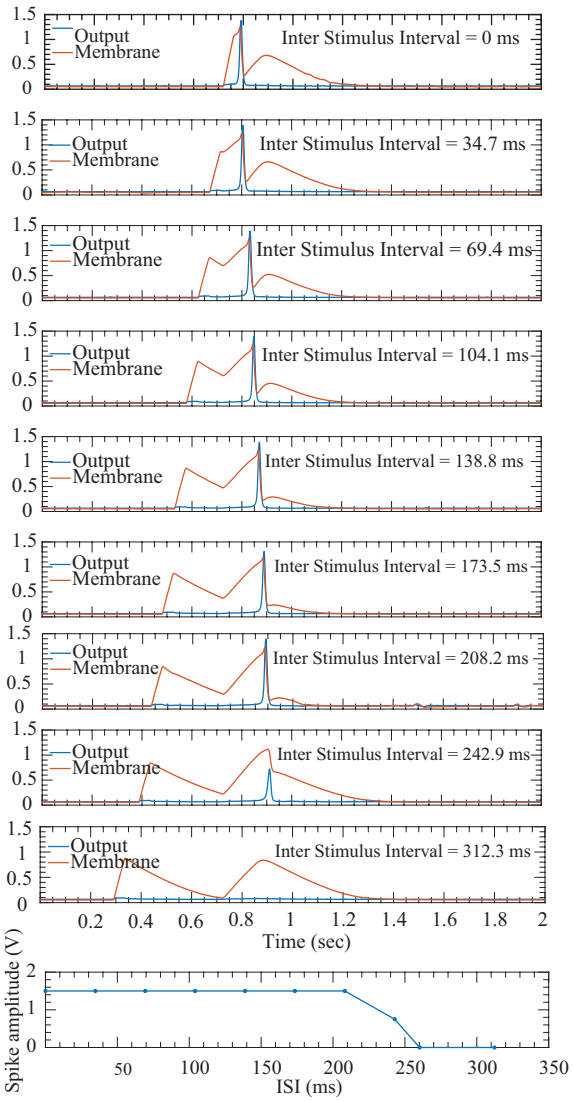


**Supplementary Figure 18** Comprehensive dataset for coincidence detection across inter-stimulus intervals (ISIs). Membrane voltage traces for multiple ISIs show the neuron's transition from successful integration (coincidence detection) to signal separation. Neuronal response disappears beyond an ISI of 260.25 ms.